Electrochimica Acta 56 (2011) 4876–4881

Contents lists available at ScienceDirect

Electrochimica Acta

journal homepage: www.elsevier.com/locate/electacta

Molten hydroxides synthesis of hierarchical cobalt oxide nanostructure and its application as anode material for lithium ion batteries

Minwei Xu, Fei Wang*, Mingshu Zhao, Sen Yang, Xiaoping Song**

MOE Key Laboratory for Nonequilibrium Synthesis and Modulation of Condensed Matter, School of Science, Xi'an Jiaotong University, Xi'an 710049, PR China

ARTICLE INFO

Article history:
Received 14 January 2011
Received in revised form 24 February 2011
Accepted 4 March 2011
Available online 17 March 2011

Keywords:
Cobalt oxide
Nanostructure
Anode
Lithium ion battery

ABSTRACT

Hierarchical Co_3O_4 nanostructure is synthesized via a self-assembled process in molten hydroxides. The morphologies, crystal structures and the phase transformation processes are analyzed by field-emission scanning electron microscopy, transmission electron microscopy, and X-ray diffraction. As an anode material for lithium ion batteries, the hierarchical Co_3O_4 exhibit an initial capacity of 1336 mAh g^{-1} and a stable capacity of 680 mAh g^{-1} over 50 cycles. More importantly, high rate capability is obtained at different current densities between 140 and 1120 mA g^{-1}. The improved electrochemical performance of Co_3O_4 could be attributed to the unique hierarchical nanostructure.

1. Introduction

Cobalt oxide (Co_3O_4) has attracted increasing attention due to its unique properties and potential applications in diverse fields, such as catalysis, gas sensors and field-emission devices [1–4]. In addition, Co_3O_4 is also regarded as a promising alternative anode material for rechargeable lithium ion batteries [5], which exhibits a high theoretical capacity of 890 mAh g^{-1}. However, the severe volume expansion/contraction associated with Li^+ insertion and extraction processes causes the pulverization of electrode and leads to a rapid deterioration in capacity [6,7]. To overcome this intrinsical drawback, it is suggested that hybridizing Co_3O_4 with carbon material is an effective approach [8,9]. Nevertheless, this strategy sacrifices the capacity of Co_3O_4 due to the introduction of carbon. Moreover, the reliable synthesis of well-designed Co_3O_4/carbon nanocomposites remains a challenge. In general, it is well accepted that the morphology of Co_3O_4 nanostructures can greatly affect their electrochemical properties [10,11]. Over the past few years, intensive researches have been devoted to the synthesis of novel Co_3O_4 nanostructures, which reveals a promising way to improve the electrochemical performances of Co_3O_4 anodes. For instance, various Co_3O_4 nanostructures such as nanotubes [12,13], octahedral cages [14], mesoporous needles [15], hollow structures [16,17] and pompon-like microspheres [18] have been reported and exhibit the enhanced electrochemical properties. However, there should be still much space for progress to achieve the satisfactory cycle performance and high rate capability for the practical application of Co_3O_4 anodes, particularly in terms of novel morphology and controlled synthesis. In particular, hierarchical architectures assembled by low-dimensional building blocks have been considered to be the ideal nanostructures for enhanced electrochemical performances [19–21]. The improved properties could be mainly attributed to the loose structure, large surface area, and shortened Li^+ diffusion distance.

The molten-salt synthesis method is one of the simple, versatile, and cost-effective approaches for obtaining oxide nanostructures [22]. Recently, Wang and co-workers demonstrated the feasibility of a composite-hydroxide-mediated (CHM) approach to synthesize oxide nanostructures [23]. This method is based on the reactions of raw materials in eutectic hydroxide melts and it provides a one-step, convenient, low cost, nontoxic and mass-production route for various oxide nanostructures. Up to now, a wide range of complex oxides, hydroxides and simple oxides has been synthesized by CHM approach, including $BaTiO_3$, $CoFe_2O_4$, $Pb_2V_2O_7$, Niobate, $La(OH)_3$, CuO, CeO_2, etc. [24–28]. However, to the best of our knowledge, there is few works to report the synthesis of Co_3O_4 nanostructures via CHM approach.

Herein, we adopt the so-called CHM approach to synthesize hierarchical Co_3O_4 nanostructures. It is found that the as-obtained Co_3O_4 nanostructure is assembled by extremely thin nanosheets. The reaction mechanism for the formation of Co_3O_4 nanostructure in molten hydroxides is discussed. Motivated by the unique morphology, the electrochemical properties of the Co_3O_4 nanostructure are investigated. In addition, the effect of the annealing temperature on the electrochemical performance is also presented.

* Corresponding author. Tel.: +86 29 82663034; fax: +86 29 82663034.
** Corresponding author. Tel.: +86 29 82665892; fax: +86 29 82665892.
E-mail addresses: feiwang@mail.xjtu.edu.cn (F. Wang), xpsong@mail.xjtu.edu.cn (X. Song).

0013-4686/$ – see front matter © 2011 Elsevier Ltd. All rights reserved.
doi:10.1016/j.electacta.2011.03.027

As anode material for lithium ion batteries, the hierarchical Co_3O_4 nanostructure displays superior lithium storage properties with good cycle stability and high rate capability.

2. Experimental

In a typical experiment, a teflon vessel filled with 20 g mixed hydroxides (NaOH:KOH = 51.5:48.5) was putted in a furnace and then heated up to 200 °C. When the hydroxides melted, 0.476 g $CoCl_2 \cdot 6H_2O$ was added and the mixture was stirred until a uniform suspension was obtained. It is found that the black precipitates were formed immediately. After maintaining at 200 °C for a period of time, the vessel was taken out and cooled to room temperature naturally. Then, deionized water was added to dissolve the residual hydroxides. The precipitates were harvested by centrifugation and washed thoroughly with deionized water and ethanol. Finally, Co_3O_4 samples were obtained by calcining the black precursors at 500 °C for 6 h. The heating rate was below 1 °C/min.

The structure, morphology of the products were characterized with X-ray powder diffraction (XRD, Bruke D8-Advance, Cu-Kα, λ = 0.15406 nm), field-emission scanning electron microscope (FESEM, JEOL JSM-7100F) and transmission electron microscopy (TEM, JEOL JEM-2100). The N_2 adsorption and desorption isotherm was obtained at 77 K using Physisorption Analyzer (ASAP 2020). The BET surface area was estimated using adsorption data in a relative pressure ranging from 0.06 to 0.3.

Electrochemical performance of the hierarchical Co_3O_4 nanostructure was investigated with two-electrode Swagelok cells. For working electrodes, the Co_3O_4 samples mixed with carbon black and polyvinylidene fluoride (PVDF) at a mass ratio of 70:20:10 were dispersed in N-methyl pyrrolidinone (NMP). Then, the slurry was coated uniformly onto copper foils (Φ = 10 mm) and dried in vacuum at 100 °C for 12 h. Test cells were assembled in argon filled glove box. Metallic lithium foil was used as counter electrode. The electrolyte was made by dissolving 1 M $LiPF_6$ in the mixture of ethylene carbonate (EC) and diethylene carbonate (DEC) with the volume ratio of 1:1. Galvanostatical charge and discharge tests were carried out on a battery testing system (Arbin-BT2000) with the voltage range of 0.01–3.0 V (vs. Li/Li^+). Cyclic voltammograms were performed on Ametek VMC-4 electrochemical testing system between 3.0 V and 0 V at a scan rate of 0.5 mV s^{-1}.

3. Results and discussion

In this work, the mixed hydroxides are employed not only as the solvent but also as the reactant for preparing the precursors. Fig. 1a–d displays the morphological images of the precursors, which are obtained with a reaction time of 1 min (precursor A)

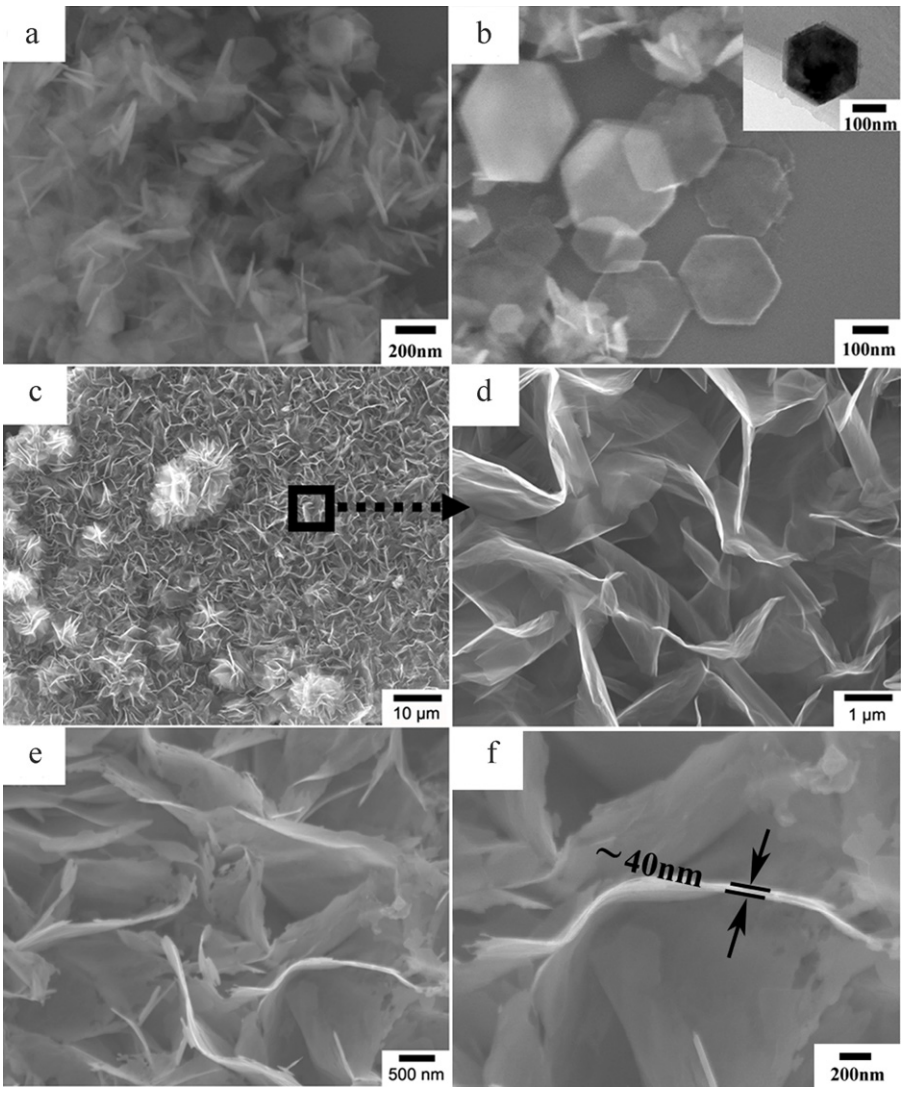

Fig. 1. Morphological images of as-synthesized precursors with a reaction time of (a and b) 1 min (precursor A), (c and d) 8 h (precursor B) and (e and f) SEM image of Co_3O_4 nanostructure produced by calcining the precursors B at 500 °C for 6 h.

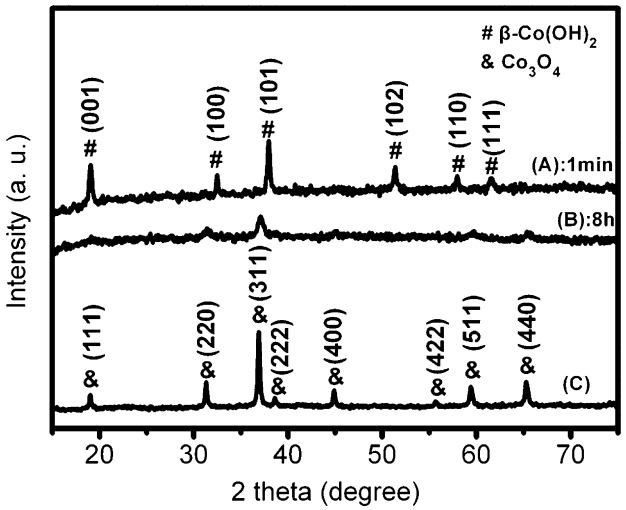

Fig. 2. XRD patterns of precursor A, B and Co_3O_4 nanostructure obtained by calcining the precursors B at 500 °C for 6 h.

and 8 h (precursor B). For precursor A obtained at the early stage, the XRD pattern (Fig. 2A) can be indexed to hexagonal β-$Co(OH)_2$ (JCPDS No. 30-0443). The formation of β-$Co(OH)_2$ is described as follows:

$$CoCl_2 + 2NaOH/KOH \rightarrow Co(OH)_2 + 2NaCl/KCl \quad (1)$$

It is well known that β-$Co(OH)_2$ nanocrystals are usually obtained in plate morphology due to its brucite-like layered structure [29]. As showed in Fig. 1a–b, a large amount of β-$Co(OH)_2$ plates are observed. These plates are hexagonal. The size of the plates is several hundreds nanometers and the thickness is estimated to be less than 50 nm. Increasing the reaction time to 8 h (precursor B), biggish nanosheets instead of nanoplates is obtained (Fig. 1c–d). More interestingly, these nanosheets vertically assemble into hierarchical nanostructure in large-scale. The nanosheets are convolute spontaneously and present a large free space naturally. Fig. 2B shows the XRD pattern of precursor B, the broad and weak peaks indicate that it is poorly crystallized. Moreover, some diffraction peaks of cubic Co_3O_4 are also found. These results indicate the oxidation from Co (II) to Co (III) in molten hydroxides by the uptake of oxygen [30]:

$$6Co(OH)_2 + O_2 \rightarrow 2Co_3O_4 + 6H_2O \quad (2)$$

In addition, it should be pointed out that a trace of flower-like spheres can also be found in Fig. 1c. The details of the self-assembled processes are still not clear and further works on it is underway.

Fig. 1e–f shows the SEM images of Co_3O_4 nanostructure, which was obtained by calcining precursor B in air at 500 °C for 6 h. From it we can see that no substantial change is observed and the morphology of precursor B is preserved after the heat treatment. The thickness is estimated to be about 40 nm. Due to the thermal decomposition, the obtained Co_3O_4 exhibits flawed nanosheet morphology. The XRD curve, as shown in Fig. 2C, indicates that the hierarchical nanostructure consists of well-crystallized Co_3O_4. All the diffraction peaks can be indexed to a cubic structure of Co_3O_4 (JCPDS No. 74-2120). Fig. 3a shows the TEM images of Co_3O_4 nanostructures. The SAED pattern (Fig. 3b) demonstrates that the Co_3O_4

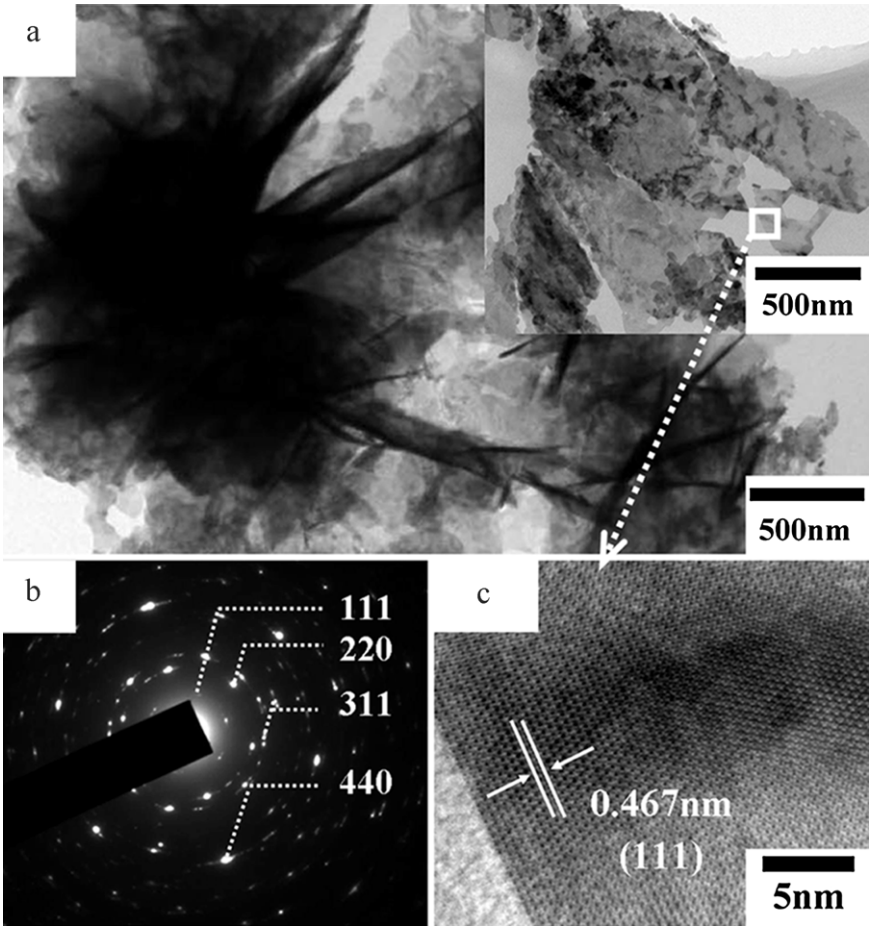

Fig. 3. (a) TEM images, (b) SAED pattern and (c) HRTEM image of hierarchical Co_3O_4 nanostructure.

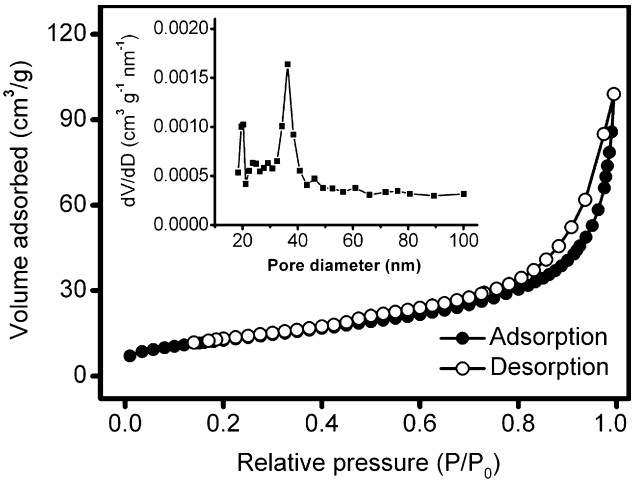

Fig. 4. N_2 adsorption–desorption isotherm of the Co_3O_4 nanostructure after calcinations at 500 °C.

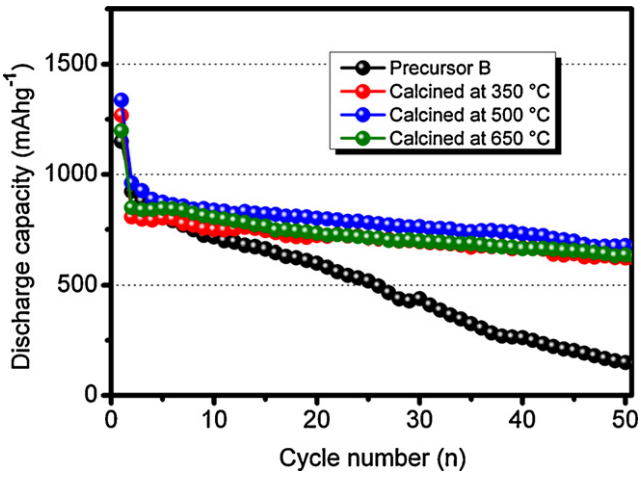

Fig. 6. The cycle performance of hierarchical Co_3O_4 nanostructure obtained at different temperature.

nanostructures are polycrystalline. The diffraction rings pointed out by white lines can be indexed as (1 1 1), (2 2 0), (3 1 1) and (4 4 0) planes of cubic Co_3O_4, respectively. HRTEM image exhibits the clear lattice fringes with a spacing of 0.467 nm, which corresponds to the (1 1 1) planes of cubic Co_3O_4.

The surface area of the hierarchical Co_3O_4 nanostructure is measured by Brunauer–Emmett–Teller (BET) method. The N_2 adsorption–desorption isotherms at 77 K are shown in Fig. 4, with the insets showing the pore size distribution by Barrett–Joyner–Halenda (BJH) method. It is found that the overall hierarchical Co_3O_4 have a BET surface area of 45.6 $m^2\ g^{-1}$ and a pore volume of 0.153 $cm^3\ g^{-1}$. The isotherm is characteristic of a type IV with a type H3 hysteresis loop, revealing that the Co_3O_4 sample is composed of aggregates of sheet-like particles forming slit-like pores [31]. It is well correspondence with the previous microscopy findings in Fig. 1e–f.

The electrochemical reaction processes are investigated by cyclic voltammograms. Fig. 5a shows the CV curves of the hierarchical Co_3O_4 at a scan rate of 0.5 mV s^{-1}. During the first cathodic scan, only one broad peak near 0.66 V could be observed. Compared to the initial cycle, a decrease of peak intensity and a shift of the potential to the positive direction are revealed in the subsequent cycles. This cathodic peak corresponds to a multistep electrochemical reaction, which is generally attributed to the reduction of Co (III) to Co (II) and metal Co [32]. In the anodic scans, one peak in the range of 1.9–2.5 V is recorded, which are ascribed to the reversible oxidation of metal Co to cobalt oxide. Except for the first cycle, the following CV curves are similar, which demonstrate the good cycle stability of the electrode during the discharge–charge cycles. The electrochemical reaction of Li with Co_3O_4 can be expressed as follows [33,34]:

$$Co_3O_4 + 8Li^+ + 8e^- \leftrightarrow 4Li_2O + 3Co \quad (3)$$

Fig. 5b displays the discharge–charge curves of the hierarchical Co_3O_4 nanostructure measured between 0.01 and 3.0 V at a current density of 180 mA g^{-1}. The discharge–charge behaviors and the curve plateaus are corresponding well with the cathodic and anodic peaks in Fig. 5a. Since the second cycle, the curves are similar with a gradually decrease in capacity. Usually, Li-driven formation of nanoscale Co dispersed into Li_2O matrix goes with a series of irreversible reactions during the first discharge process such as the decomposition of electrolyte and the formation of solid electrolyte interphase (SEI) films [35]. These irreversible reactions result in large initial irreversible capacity and low coulombic efficiency. In present case, the Co_3O_4 electrode exhibits the discharge capacity of 1336 mAh g^{-1} and the charge capacity of 800 mAh g^{-1} in the first cycle.

The cycle performances of the hierarchical Co_3O_4 nanostructure prepared at different temperature are shown in Fig. 6. The result shows that the annealed Co_3O_4 nanostructures exhibit the similar cycle performances. However, the precursor B exhibits the poor cycle performance with obvious capacity fade. It is believed that the oxidation from Co (II) to Co (III) in molten hydroxides is a complex reaction process. The side products, such as amorphous CoOOH, $Co(OH)_3$ may be formed in precursor B. Hence, the thermal-treatment ensures the good phase purity of the hierarchical Co_3O_4

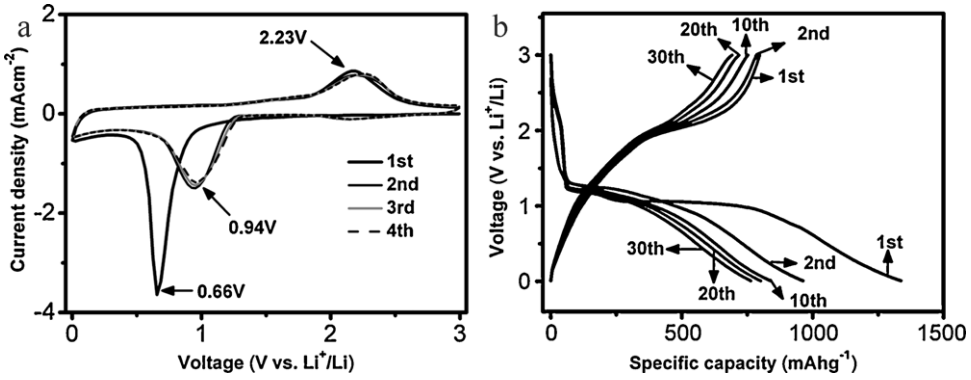

Fig. 5. (a) The first four cyclic voltammogram curves for Co_3O_4 nanostructure at a scan rate of 0.5 mV s^{-1} and (b) the typical charge–discharge profiles of Co_3O_4 nanostructures in the appointed cycles.

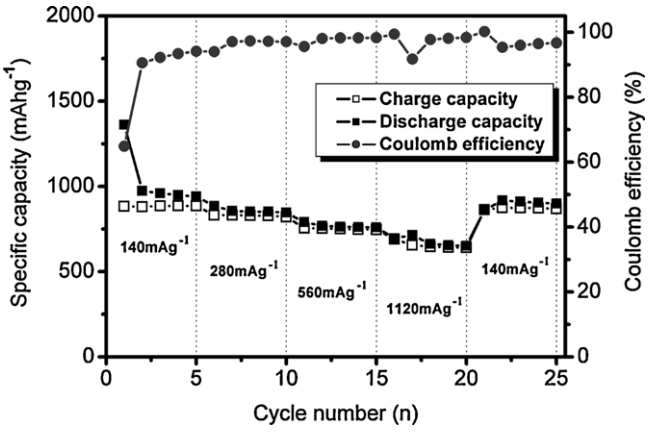

Fig. 7. Rate capability of hierarchical Co_3O_4 nanostructure at various current densities between 140 and 1120 mA g^{-1}.

nanostructures, which is significant for their electrochemical performance. Compared to other samples, the hierarchical Co_3O_4 nanostructure annealed at 500 °C exhibits a higher discharge capacity. Moreover, the electrode reveals a slow capacity fading and achieves a stable reversible capacity above 680 mAh g^{-1} over 50 cycles.

Motivated by the extremely thin thickness of single Co_3O_4 nanosheet, the rate capability of the hierarchical Co_3O_4 nanostructure obtained at 500 °C is studied and presented in Fig. 7. The Initial charge capacities of 885 mAh g^{-1}, 832 mAh g^{-1}, 757 mAh g^{-1} and 680 mAh g^{-1} are observed at the different current densities of 140 mA g^{-1}, 280 mA g^{-1}, 560 mA g^{-1} and 1120 mA g^{-1}, respectively. The coulomb efficiency rises rapidly from 65.1% to 94.2% within five cycles. Then, it remains above 97.0% in the following cycles even at high current density. When the current density returns to 140 mA g^{-1} after 20 cycles, the electrode recovers its original capacity.

As compared to many reported Co_3O_4 nanoparticles, nanocubes and porous microspheres [18,33,36,37], the hierarchical Co_3O_4 nanostructure exhibit better electrochemical performance. The improved performance may be attributed to the unique hierarchical feature of Co_3O_4 nanostructure. On the one hand, the large area between the Co_3O_4 nanosheets can alleviate the influence of the volume change during lithiation/delithiation processes, which generate good capacity retention. Fig. 8 shows the SEM image of the hierarchical Co_3O_4 nanostructures after 50 cycles. Compared with Fig. 1f, it can be see that the morphology of Co_3O_4 nanosheet partially remained after the lithiation/delithiation cycles. On the other hand, the primary Co_3O_4 nanosheet, which is extremely thin in thickness, can effectively shorten the diffusion distance of Li^+. Therefore, the rate capability is improved and the large specific capacities are achieved at high current densities. The enhanced cycle performance as well as the high rate capability of the obtained Co_3O_4 nanostructure demonstrated that the synthesis of hierarchical architectures is an effective way to improve the electrochemical performance of Co_3O_4 anode materials.

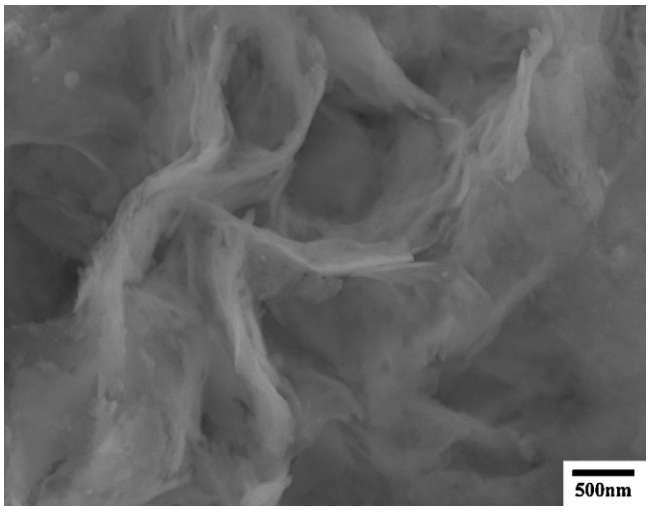

Fig. 8. SEM image of the hierarchical Co_3O_4 nanostructure after 50 cycles.

4. Conclusions

In summary, novel Co_3O_4 nanostructures with a hierarchical architecture have been prepared via self-assemble of nanosheet blocks in molten hydroxides. It is believed that the reaction mechanism includes the following processes: (1) the formation of β-$Co(OH)_2$ nanoplates; (2) the morphology evolution and self-assemble of nanoplates to hierarchical architecture going with the oxidation of $Co(OH)_2$; and (3) the transformation of the precursor to well crystallized Co_3O_4 nanostructures by heat treatment. When tested as anode materials for lithium ion battery, the hierarchical Co_3O_4 exhibited high reversible capacity, good cycle performance, and high rate capability.

Acknowledgements

This work was supported by National Natural Science Foundation of China (51002117 and 51071117), the National Basic Research Program of China (2010CB635101) and Fundamental Research Funds for the Central Universities (0109-08141012).

References

[1] H. Tuysuz, M. Comotti, F. Schuth, Chem. Commun. 34 (2008) 4022.
[2] C.Y. Ma, Z. Mu, J.J. Li, Y.G. Jin, J. Cheng, G.Q. Lu, Z.P. Hao, S.Z. Qiao, J. Am. Chem. Soc. 132 (2010) 2608.
[3] B.Y. Geng, F.M. Zhan, C.H. Fang, N. Yu, J. Mater. Chem. 18 (2008) 4977.
[4] T. Yu, Y.W. Zhu, X.J. Xu, Z.X. Shen, P. Chen, C.T. Lim, J.T.L. Thong, C.H. Sow, Adv. Mater. 17 (2005) 1595.
[5] P. Poizot, S. Laruelle, S. Grugeon, L. Dupont, J.M. Tarascon, Nature 407 (2000) 496.
[6] Y.M. Kanga, M.S. Songa, J.H. Kim, H.S. Kima, M.S. Park, J.Y. Lee, H.K. Liu, S.X. Dou, Electrochim. Acta 50 (2005) 3667.
[7] Y. Lu, Y. Wang, Y.Q. Zou, Z. Jiao, B. Zhao, Y.Q. He, M.H. Wu, Electrochem. Commun. 12 (2010) 101.
[8] Z.S. Wu, W.C. Ren, L. Wen, L.B. Gao, J.P. Zhao, Z.P. Chen, G.M. Zhou, F. Li, H.M. Cheng, ACS Nano 4 (2010) 3187.
[9] G.X. Wang, X.P. Shen, J.N. Yao, D. Wexler, J.H. Ahn, Electrochem. Commun. 11 (2009) 546.
[10] T. Zhu, J.S. Chen, X.W. Lou, J. Mater. Chem. 20 (2010) 7015.
[11] J.S. Chen, T. Zhu, Q.H. Hu, J.J. Gao, F.B. Su, S.Z. Qiao, X.W. Lou, ACS Appl. Mater. Interfaces 2 (2010) 3628.
[12] W.Y. Li, L.N. Xu, J. Chen, Adv. Mater. 15 (2005) 851.
[13] N. Du, H. Zhang, B.D. Chen, J.B. Wu, X.Y. Ma, Z.H. Liu, Y.Q. Zhang, D.R. Yang, X.H. Huang, J.P. Tu, Adv. Mater. 19 (2007) 4505.
[14] X. Wang, L.J. Yu, X.L. Wu, F.L. Yuan, Y.G. Guo, Y. Ma, J.N. Yao, J. Phys. Chem. C 113 (2009) 15553.
[15] X.W. Lou, D. Deng, J.Y. Lee, L.A. Archer, J. Mater. Chem. 18 (2008) 4397.
[16] S.L. Chou, J.Z. Wang, H.K. Liu, S.X. Dou, J. Power Sources 182 (2008) 359.
[17] Y. Sun, X.Y. Feng, C.H. Chen, J. Power Sources 196 (2011) 784.
[18] B. Guo, C.S. Li, Z.Y. Yuan, J. Phys. Chem. C 114 (2010) 12805.
[19] Y.G. Li, B. Tan, Y.Y. Wu, Nano Lett. 8 (2008) 265.
[20] X. Wang, X.L. Wu, Y.G. Guo, Y.T. Zhong, X.Q. Cao, Y. Ma, J.N. Yao, Adv. Funct. Mater. 20 (2010) 1680.
[21] X.H. Xia, J.P. Tu, J.Y. Xiang, X.H. Huang, X.L. Wang, X.B. Zhao, J. Power Sources 195 (2010) 2014.
[22] Y.B. Mao, T.J. Park, F. Zhang, H.J. Zhou, S.S. Wong, Small 3 (2007) 1122.
[23] C.G. Hu, Y. Xi, H. Liu, Z.L. Wang, J. Mater. Chem. 19 (2009) 858.
[24] H. Liu, C.G. Hu, Z.L. Wang, Nano Lett. 6 (2006) 1535.
[25] C.Y. Xu, L. Zhen, R.S. Yang, Z.L. Wang, J. Am. Chem. Soc. 129 (2007) 15444.
[26] C.G. Hu, H. Liu, W.T. Dong, Y.Y. Zhang, G. Bao, C.S. Lao, Z.L. Wang, Adv. Mater. 19 (2007) 470.

[27] X. Wang, C.G. Hu, H. Liu, G.J. Du, X.S. He, Y. Xi, Sens. Actuators B: Chem. 144 (2010) 220.
[28] C.G. Hu, Z.W. Zhang, H. Liu, P.X. Gao, Z.L. Wang, Nanotechnology 17 (2006) 5983.
[29] X.W. Lou, D. Deng, J.Y. Lee, J. Feng, L.A. Archer, Adv. Mater. 20 (2008) 258.
[30] J.Q. Wang, G.D. Du, R. Zeng, B. Niu, Z.X. Chen, Z.P. Guo, S.X. Dou, Electrochim. Acta 55 (2010) 4805.
[31] C. Wang, Y. Zhou, M.Y. Ge, X.B. Xu, Z.L. Zhang, J.Z. Jiang, J. Am. Chem. Soc. 132 (2010) 46.
[32] D. Larcher, G. Sudant, J.B. Leriche, Y. Chabre, J.M. Tarascon, J. Electrochem. Soc. 149 (2002) A234.
[33] D. Barreca, M. Cruz-Yusta, A. Gasparotto, C. Maccato, J. Morales, A. Pozza, C. Sada, L. Sanchez, E. Tondello, J. Phys. Chem. C 114 (2010) 10054.
[34] L. Tian, H.L. Zou, J.X. Fu, X.F. Yang, Y. Wang, H.L. Guo, X.H. Fu, C.L. Liang, M.W. Wu, P.K. Shen, Q.M. Gao, Adv. Funct. Mater. 20 (2010) 617.
[35] P. Poizot, S. Laruelle, S. Grugeon, L. Dupont, J.-M. Tarascon, J. Power Sources 97/98 (2001) 235.
[36] J. Zheng, J. Liu, D.P. Lv, Q. Kuang, Z.Y. Jiang, Z.X. Xie, R.B. Huang, L.S. Zheng, J. Solid State Chem. 183 (2010) 600.
[37] M.M. Rahman, J.Z. Wang, X.L. Deng, Y. Li, H.K. Liu, Electrochim. Acta 55 (2009) 504.